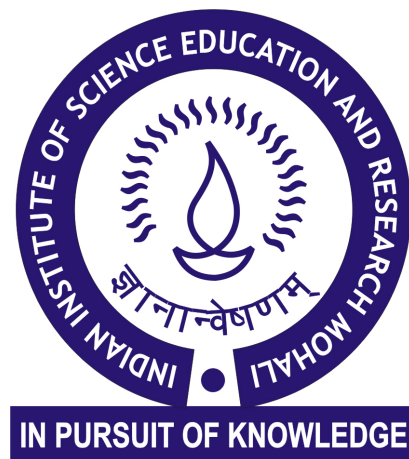


Proposed Study of Magnetic films using Magnetocapacitance

Dhruv Mittal
Roll No: MS15075

*A dissertation submitted for the partial fulfilment
of BS-MS dual degree in Science*

Under the guidance of
Dr. Ananth Venkatesan



Indian Institute of Science Education and Research Mohali
June 2020

Certificate of Examination

This is to certify that the dissertation titled **Proposed Study of Magnetic films using Magnetocapacitance** submitted by **Dhruv Mittal** (Reg. No. MS15075) for the partial fulfillment of BS-MS dual degree programme of the Institute, has been examined by the thesis committee duly appointed by the Institute. The committee finds the work done by the candidate satisfactory and recommends that the report be accepted.

Dr. Kamal P. Singh

Dr. Samir K. Biswas

Dr. Ananth Venkatesan

(Supervisor)

Dated: 15.06.2020

Declaration

The work presented in this dissertation has been carried out by me under the guidance of Dr. Ananth Venkatesan at the Indian Institute of Science Education and Research Mohali.

This work has not been submitted in part or in full for a degree, a diploma, or a fellowship to any other university or institute. Whenever contributions of others are involved, every effort is made to indicate this clearly, with due acknowledgement of collaborative research and discussions. This thesis is a bonafide record of original work done by me and all sources listed within have been detailed in the bibliography.

Dhruv Mittal
(Candidate)

Dated: June 13, 2020

In my capacity as the supervisor of the candidate's project work, I certify that the above statements by the candidate are true to the best of my knowledge.

Dr. Ananth Venkatesan
(Supervisor)

Acknowledgement

First and foremost, I would like to thank my thesis supervisor Dr. Ananth Venkatesan, for his support and supervision, throughout the year and especially during the uncertain times of the pandemic. I would also like express my heartfelt gratitude to Shelender Kumar for always being there to help me, guide me and give me the mental strength to continue with my work. I would also like to thank my lab mates Shyam, Dr. Radhikesh, Anubhav, Himanshu, Vivek and Pankaj for the creating a friendly and fun environment to work in.

Dhruv Mittal
MS15075
IISER Mohali.

List of Figures

| | | |
|-----|---|----|
| 1.1 | Density of States of a 2DEG in a magnetic field ^[1] | 2 |
| 1.2 | Capacitance value changes in sharp correspondence to the DOS ^[2] | 3 |
| 1.3 | Capacitance minima at Hall plateaus in QHE regime ^[3] | 3 |
| 1.4 | The two possible spin orientations of an electron. | 4 |
| 2.1 | Equivalent circuit of MIM capacitor ^[8] | 5 |
| 2.2 | Inverse areal capacitance versus dielectric thickness for Pd-AlO _x (d) -Al ^[11] | 6 |
| 2.3 | Normalised change in capacitance versus H^2 for Pd-AlO _x -Al ^[11] | 7 |
| 2.4 | DOS for up and down electrons in the Stoner model of itinerant ferromagnetism ^[15] | 8 |
| 2.5 | DOS for up and down electrons in the model of itinerant ferromagnetism considering bandwidth changes and spin-splitting of bands ^[17] | 9 |
| 2.6 | Contour plots of susceptibility, and magnetocapacitance which is proportional to the quantity f_2 in the calculations. n_0 is the electron concentration and j is the parameter describing strength of interactions ^[16] | 9 |
| 2.7 | Linear decrease in Magnetic susceptibility against hydrogen concentration x in PdH _{x} at different temperatures ^[18] | 10 |
| 2.8 | (a) Schematic drawing of H ₂ interacting with the MIS device. (b) Voltage shift caused by dipole layer induced by hydrogen at the metal- insulator interface ^[20] | 11 |
| 3.1 | Schematic of a standard Thermal evaporation system | 14 |
| 3.2 | Schematic of a standard E-beam evaporation system | 15 |
| 3.3 | Schematic of deposition of SiO ₂ by a reactive e-beam evaporation ^[23] | 16 |
| 3.4 | Schematic of deposition of Al ₂ O ₃ by a reactive sputtering of Al reported by Palaniyappan et al ^[26] | 17 |

| | | |
|-----|--|----|
| 3.5 | Schematic of MIM structure with circular top electrode. | 17 |
| 3.6 | Schematic of MIM structure with cross configuration. | 18 |
| 3.7 | MIM structures fabricated by shadow masking with stencils. | 18 |
| 3.8 | Shadow masking with Teflon tape. | 19 |
| 3.9 | MIM structure fabricated in cross configuration using e-beam lithography. . | 19 |
| 4.1 | Impedance vs Frequency for MIM fabricated with AlO_x film as the dielectric. | 21 |
| 4.2 | Capacitance vs AC Voltage for MIM with AlO_x film as the dielectric. . . . | 22 |

Contents

| | |
|---|------------|
| Acknowledgement | i |
| List of Figures | iv |
| Abstract | vii |
| 1 Introduction | 1 |
| 1.1 Density of states | 1 |
| 1.2 Capacitance as a measure of Density of States | 2 |
| 1.3 Electrical Screening due to e-e interactions | 3 |
| 1.4 Magnetocapacitance | 4 |
| 2 Magnetocapacitance in MIM structures | 5 |
| 2.1 Interfacial capacitance | 5 |
| 2.2 Pd-AlO _x -Al | 7 |
| 2.3 Theoretical models | 7 |
| 2.3.1 Stoner Model | 7 |
| 2.3.2 Generalized tight-binding model | 8 |
| 2.4 Proposed systems to be studied | 10 |
| 2.4.1 Palladium-hydrogen system | 10 |
| 2.4.2 Magnetic phases and phase transitions | 11 |
| 3 Experiment | 13 |
| 3.1 Fabrication | 13 |
| 3.1.1 Cleaning the substrate | 13 |
| 3.1.2 Deposition Methods | 14 |
| 3.1.3 Design | 17 |

| | | |
|----------|-------------------------------------|-----------|
| 3.1.4 | Shadow Masking | 18 |
| 3.1.5 | Electron-beam lithography | 19 |
| 3.1.6 | Contacts | 19 |
| 3.2 | Measurements | 20 |
| 3.2.1 | Leakage Current | 20 |
| 3.2.2 | Impedance Measurement | 20 |
| 4 | Observations and Conclusions | 21 |
| | Bibliography | 23 |

Abstract

The interplay between spin and charge is one of the most discussed topics in condensed matter physics today, because of the fundamental physics as well as practical importance. Spintronics is one such field which uses the spin of electrons to make novel devices. Usually, experiments in such studies are based on measurement of transport phenomenon. In this thesis, a different technique is proposed which uses only 2 probes and examines changes in capacitance in thin film parallel plate capacitive metal/insulator/metal (MIM) structures with the application of a magnetic field (Magnetocapacitance). It is expected that changes in the magnetic properties of the metal electrodes should reflect in the magnetocapacitance.

In the introduction important concepts are explained. The second chapter talks about magnetocapacitance in MIM capacitive structures, the theoretical approaches to model magnetocapacitance, and also explains the proposed studies. The third chapter discusses the experiments that have been so far with a focus on optimising the process to fabricate these MIM structures. In the last chapter the observations and conclusions, of the fabrication experiments done, are talked about.

Chapter 1

Introduction

Lower dimensional structures like thin films, 1-D wires, and quantum dots often show interesting and useful properties markedly distinct from their bulk counterparts due to symmetry reduction, geometric confinement of electrons, and boundary effects. Thin films, in particular, have been of great interest. While strictly speaking they are not 2-dimensional, their simple geometry facilitates a detailed exploration of the connection between atomistic details and macroscopic physical properties.

Technological advancements over the years, have empowered us today to have a much greater control in making thin films. Atomic layer deposition, for example, helps us deposit almost defect free crystalline films. This enables us to design systematic studies to explore the rich physics of films by precisely varying thicknesses, and study and characterize interfacial, surface and bulk effects in great detail.

In this chapter some concepts essential for subsequent discussion have been explained.

1.1 Density of states

The density of states (DOS) essentially indicates the number of different states at a particular energy level which can be occupied by electrons, i.e. the number of electron states per unit volume per unit energy. Determining the DOS of a material is essential as bulk properties like specific heat, paramagnetic susceptibility, and other transport properties of conductors depend on this function [1].

1.2 Capacitance as a measure of Density of States

Although, resistivity based current driven measurements have been usually used to study transport phenomena in systems like study two-dimensional electronic systems, studies have shown that capacitance measurements can be used to study electronic properties. Quantum Hall Effect (QHE) in 2DEG shows a magnetic field dependent resistivity which is indicative of the magnetic field dependence of Density of states i.e. the existence of Landau levels shown in Fig. 1.1.

Kaplit et al showed the oscillatory behaviour of capacitance (Fig. 1.2) measured between a 2DEG and the gate electrode due to the Landau levels [2]. Minima have also been observed (Fig. 1.3) in capacitance corresponding to the plateaus in hall resistance [3].

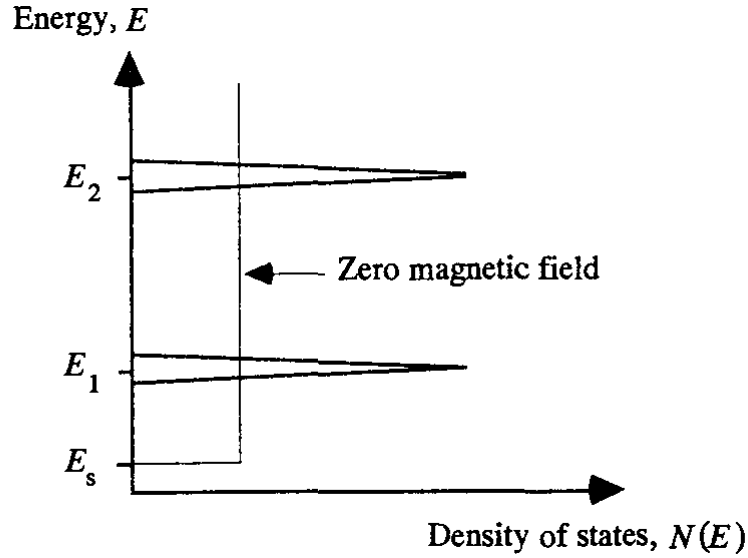


Figure 1.1: Density of States of a 2DEG in a magnetic field ^[1].

In fact, capacitance measurements are particularly well suited to determining DOS since the differential capacitance is directly related to the thermodynamic density of states (N_{TD}) [4]. For the case of the metal-insulator-semiconductor and heterostructure capacitors of area A the measured capacitance (C) is the series combination of the capacitance of the 2DEG and the capacitance of the dielectric between the electrode and the 2DEG (C_0) [5].

$$N_{TD} = (\partial n / \partial \mu) \quad (1.1)$$

$$C^{-1} = C_0^{-1} + (e^2 A N_{TD})^{-1} \quad (1.2)$$

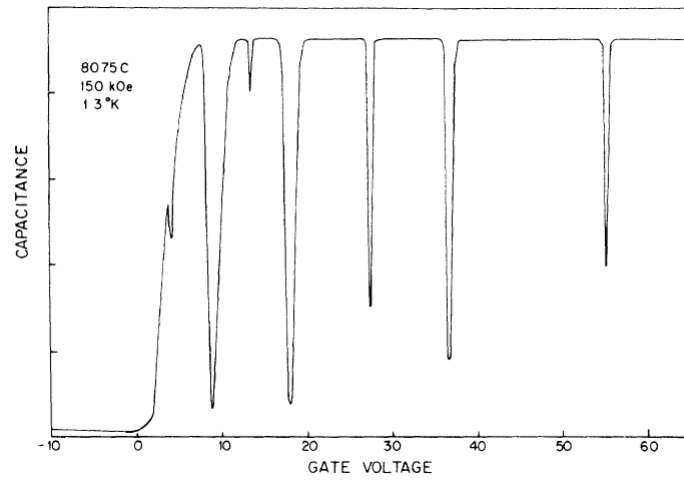


Figure 1.2: Capacitance value changes in sharp correspondence to the DOS [2].

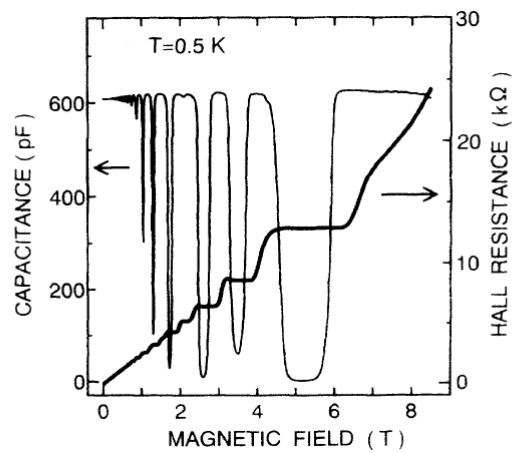


Figure 1.3: Capacitance minima at Hall plateaus in QHE regime [3].

1.3 Electrical Screening due to e-e interactions

Screening is the damping of electric fields caused by the presence of mobile charge carriers. This is caused by the rearrangement of charge carriers in electronic conductors to minimize energy and carried out by Coulomb interactions between them [6].

This screening is characterized by a Thomas Fermi screening length (λ_{TF}) over which the electric potential exponentially decays out. The DOS at the Fermi surface determines the linear screening of an external potential in a metal [7]. In the case of a smooth potential λ_{TF} relates to the DOS:

$$\lambda_{TF}^{-2} = e^2 N(\varepsilon_F) / \epsilon_0 \quad (1.3)$$

1.4 Magnetocapacitance

Spin is an additional degree of freedom that quantum particles like electrons possess. Electrons are spin half particles, i.e., they can have possible spin orientations (Fig. 1.4 : spin up and spin down).

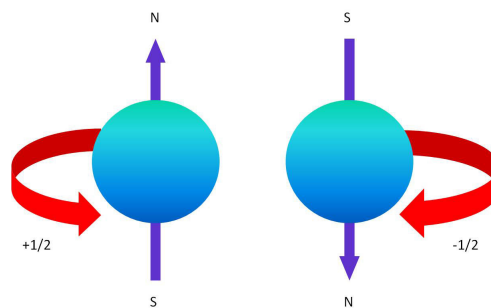


Figure 1.4: The two possible spin orientations of an electron.

Image Source: www.cnrs.fr

The interplay between spin and charge is one of the most discussed topics in condensed matter physics today, because of the fundamental physics as well as practical importance. This interplay results in the magnetoelectric effect in solids which is essentially electric field inducing magnetization and magnetic field inducing electrical polarization.

When an electric field is applied, screening charges buildup on the surface of the metal. This influences the surface magnetization of the metal. Further an applied magnetic field manipulates the screening charges which can be observed as changes in the capacitance. This is known as the magnetocapacitance effect. Thus by measuring magnetocapacitance we can gain insight into these effects.

Chapter 2

Magnetocapacitance in MIM structures

Capacitive structures have found many microelectronic applications: Metal–insulator– semiconductor (MIS) in field effect transistors (FETs), charge storage capacitors in dynamic random-access memories, and metal–insulator–metal (MIM) capacitors in RF and analog/ mixed devices.

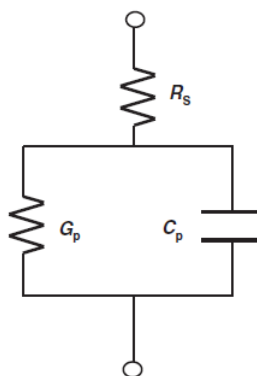


Figure 2.1: Equivalent circuit of MIM capacitor [8].

2.1 Interfacial capacitance

For a parallel plate capacitor with a bulk dielectric, the capacitance can be written as

$$C = \kappa\epsilon_0 A/d \quad (2.1)$$

where κ is the permittivity of the bulk dielectric, A is the area, and d is the thickness of the dielectric layer. Going by this classical approach, we should expect the inverse capacitance

(C^{-1}) to approach zero as d approaches zero. However experiments have shown a large non zero intercept (Fig. 2.2) on the inverse capacitance axis when plotted versus d [9]–[11].

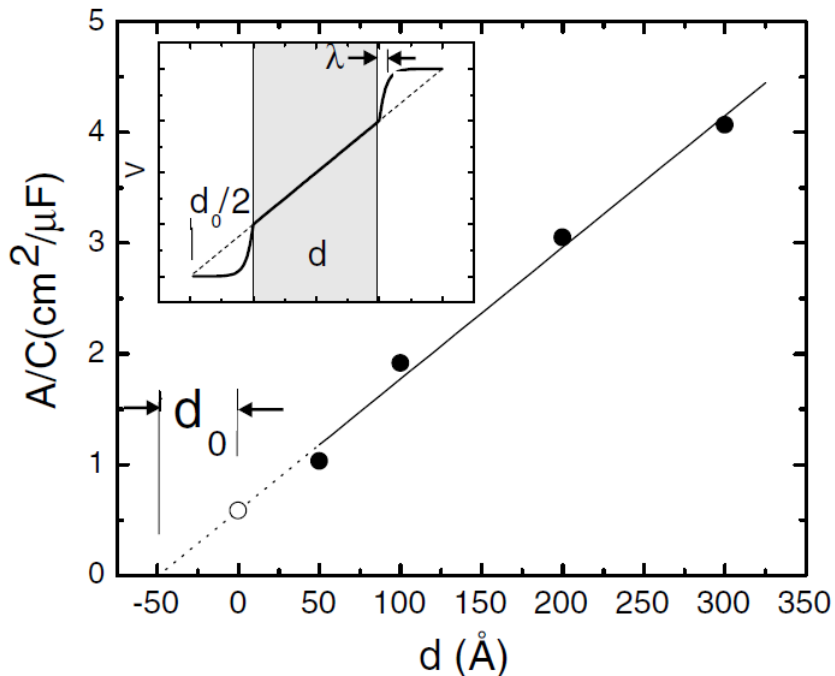


Figure 2.2: Inverse areal capacitance versus dielectric thickness for Pd-AlO_x(d) -Al [11].

This clearly indicates that capacitance in thin MIM structures depends on the bulk dielectric as well as the interfacial properties. It can be thought of as an interfacial capacitance (C_i) in series with the geometric capacitance (C_g). This C_i has been shown, by Mead, to be proportional to the electronic DOS of the electrode used [12]. Krupski's theoretical analysis showed that C_i can be attributed to the screening of electrostatic potential in the electrodes [13]. This has depicted in the inset in Fig. 2.2. To summarise the measured capacitance C_m can be understood as

$$\frac{A}{C_m} = \frac{A}{C_i} + \frac{A}{C_g} = \frac{d}{\kappa\epsilon_0} + \frac{d_0}{\kappa\epsilon_0} \quad (2.2)$$

where $d_0 = \kappa(\lambda_1 + \lambda_2)$, λ_1, λ_2 being the screening lengths in the two metallic electrodes.

2.2 Pd-AIO_x-Al

Palladium is d-transition metal with a large Pauli paramagnetic susceptibility and is described as a nearly ferromagnetic metal. McCarthy et al measured magnetocapacitance in Pd-AIO_x-Al thin film structures. The magnetocapacitance was found to decrease quadratically with the applied magnetic field (Fig. 2.3). This indicates that C_i vis-a-vis the screening length is dependent on the magnetic field.

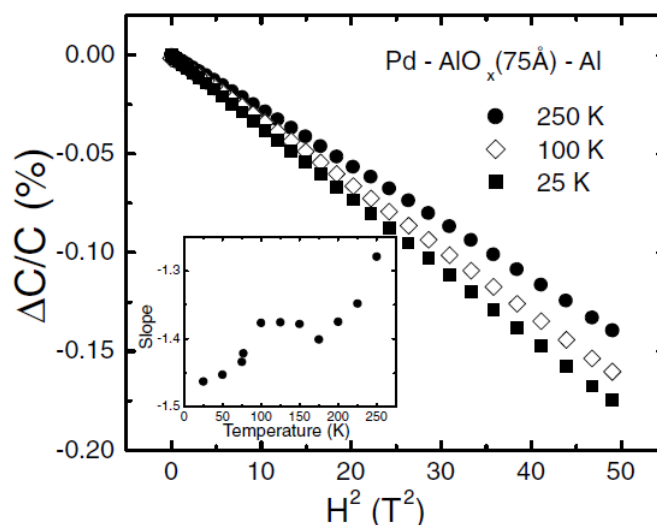


Figure 2.3: Normalised change in capacitance versus H^2 for Pd-AIO_x-Al [11].

2.3 Theoretical models

2.3.1 Stoner Model

To understand the magnetic field dependence of screening length McCarthy et al used the concept of spin dependent screening potential proposed by Zhang's theoretical work on screening in ferromagnets [14]. They argue that the magnetic field dependence of the screening length arises from the Zeeman splitting of the conduction band.

The Stoner Model of Hubbard Hamiltonian is used for describing itinerant ferromagnetism, according to which conduction band splits into two spin bands because of exchange interactions. Using this model the magnetocapacitance is calculated to be:

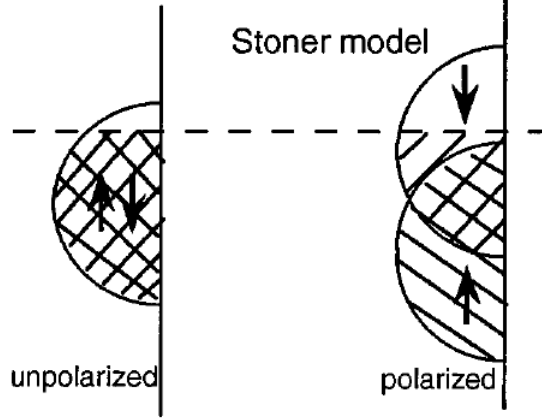


Figure 2.4: DOS for up and down electrons in the Stoner model of itinerant ferromagnetism [15].

$$\frac{C(H) - C(0)}{C(0)} = \frac{C(0)}{4\epsilon_0 A} \left[\lambda_{TF} \left(\frac{1}{1+J} \right)^{3/2} \gamma \left(\frac{\mu_B H}{1-J} \right)^2 \right] \quad (2.3)$$

where

$$\gamma = \eta + \left(\frac{2J}{1-J} \right) \left[\frac{N'(\epsilon)}{N(\epsilon)} \right]_{\epsilon_F}^2 \quad (2.4)$$

$$\eta = \left[\frac{N''(\epsilon)}{N(\epsilon)} - \left(\frac{N'(\epsilon)}{N(\epsilon)} \right)^2 \right]_{\epsilon_F} \quad (2.5)$$

Here, $N(\epsilon)$ is the DOS, ϵ_F is the Fermi energy, and $J = \frac{1}{2}UN(\epsilon_F)$ (U : onsite Coulomb interaction). This model describes the magnetocapacitance observed. This also shows that the magnetocapacitance will have a negative or positive sign based on the shape of the DOS near the Fermi energy.

2.3.2 Generalized tight-binding model

Kim et al proposed incorporating the effects of change in bandwidth along with band splitting to explain magnetocapacitance observed in Pd-AlO_x-Al [16]. This is argued based on Hirsch's proposed model to explain itinerant ferromagnetism without considering the Stoner splitting [15]. A generalized tight binding model is used which includes on-site

Coulomb interaction (U), inter-site Coulomb interaction (V), exchange interaction (J_{ex}), and pair hopping (J_{ph}). It should be noted that McCarthy et al [11] considered just the U term in the calculations.

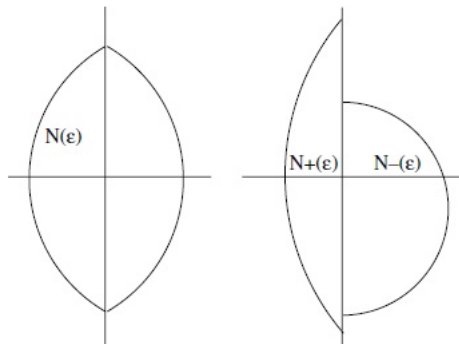


Figure 2.5: DOS for up and down electrons in the model of itinerant ferromagnetism considering bandwidth changes and spin-splitting of bands [17].

This model also describes the quadratic dependence. The study also shows that at the phase boundary between paramagnetism and ferromagnetism phases the effect of bandwidth change becomes significant, resulting in marked change in magnetocapacitance (Fig. 2.6).

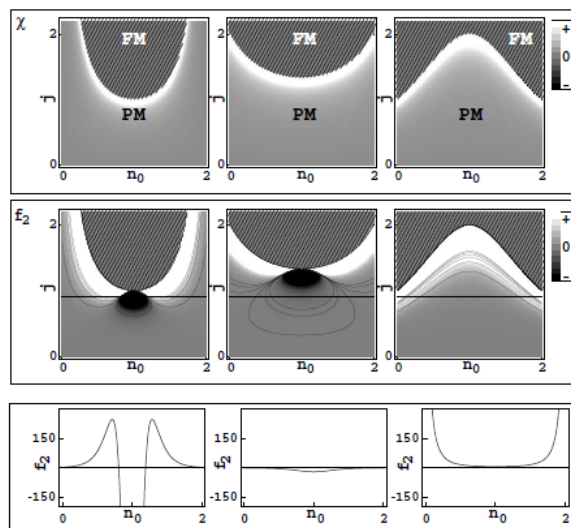


Figure 2.6: Contour plots of susceptibility, and magnetocapacitance which is proportional to the quantity f_2 in the calculations. n_0 is the electron concentration and j is the parameter describing strength of interactions [16].

2.4 Proposed systems to be studied

2.4.1 Palladium-hydrogen system

Palladium hydrogen system has been widely studied. It finds application for hydrogen storage problems. Also it serves as a good case study to investigate hydrogen induced changes in the physical properties, like DOS, band structure and Fermi surface of transition metals [9]. This shows some very interesting properties: the normal metallic state changes into a superconducting in β PdH_x ($x > 0.8$) and the linear decrease in the strong paramagnetic susceptibility with increasing hydrogen concentration (Fig. 2.7) till it completely disappears at $x = 0.6$ [18].

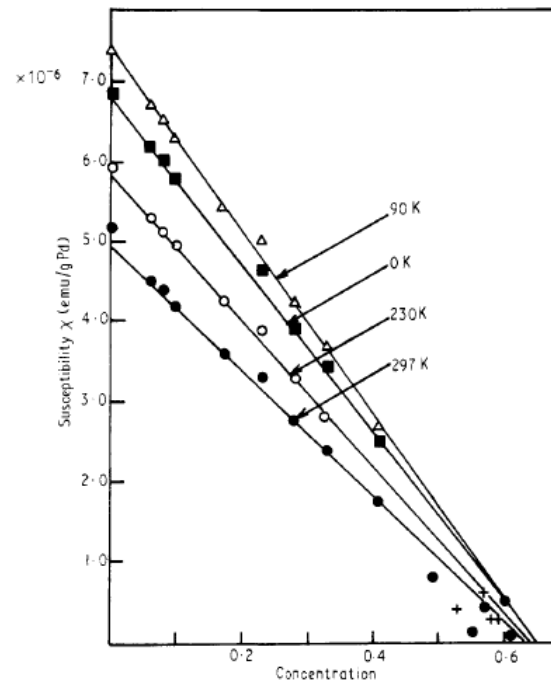


Figure 2.7: Linear decrease in Magnetic susceptibility against hydrogen concentration x in PdH_x at different temperatures [18].

The changes in physical properties have also been used to make Hydrogen sensors. Palladium (metal)-insulator-semiconductor capacitive structures show a shift in the C-V characteristics [19], [20]. Hydrogen diffuses rapidly in Pd and changes the insulator-metal interface properties (Fig.2.8). A dipole layer is induced at the interface which shows up as a voltage shift in $C - V$ characteristics.

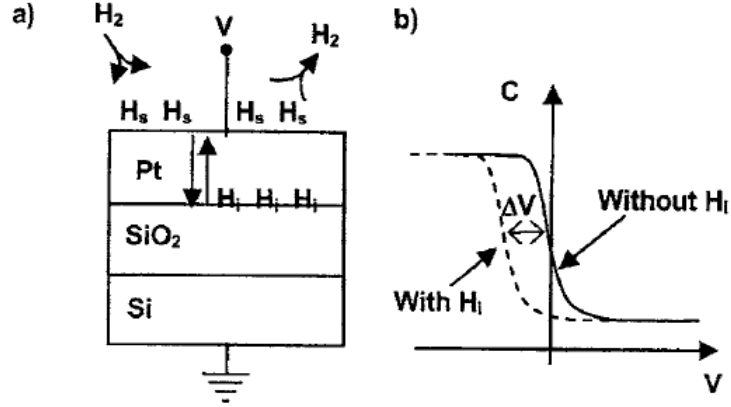


Figure 2.8: (a) Schematic drawing of H₂ interacting with the MIS device. (b) Voltage shift caused by dipole layer induced by hydrogen at the metal- insulator interface [20].

The peak of the density of states in Pd lies at an energy close to the Fermi surface [11] and thus a perturbation in the chemical potential μ may change the sign on η (Eq. 2.5) which affects the sign of the magnetocapacitance. Thus we expect magnetocapacitance of this Pd/AlO_x/Al structure to change on the introduction of hydrogen. This should give us a better insight into how hydrogen alters physical properties of Pd.

2.4.2 Magnetic phases and phase transitions

Kim et al have predicted based on the same approach based on bandwidth change and band-splitting that MIM with ferromagnetic would show a linear dependence of magnetocapacitance on magnetic field [21].

Kim et al have also predicted that a marked change in magnetocapacitance can be observed near the magnetic phase transition boundary in a ferromagnet[16]. So it is expected that magnetic phase changes in antiferromagnetic Cr film should reflect in the magnetocapacitance. The Neel temperature is around 300K which makes it feasible to observe this phase transition.

We also would like to observe changes in magnetocapacitance with respect to the superconducting transition in type 1 superconductor like Al which from being paramagnetic to perfectly diamagnetic.

Chapter 3

Experiment

The main goal of the experiment is to optimize a process to fabricate MIM structures which have a very low leakage current with the materials and deposition facilities available at the Ultra-Low Temperature Physics lab, at IISER Mohali.

In this chapter I will describe the methods that were used for the fabrication of the samples, how the contacts were made and how the basic measurements were done.

3.1 Fabrication

The MIM samples were fabricated in the clean room facility at IISER Mohali. Silicon wafers with SiO_2 film were used as substrates.

3.1.1 Cleaning the substrate

The wafer is cleaned thoroughly before starting the fabrication process. The cleaning is done in three steps:

- **Acetone cleaning:** The substrate is dipped in acetone in ultrasonic bath for 5 minutes. This removes the PMMA coating which is usually done before cutting the wafer into smaller chips.
- **Ethyl lactate cleaning:** The substrate is then dipped in ethyl lactate for 5 minutes in the ultrasonic bath. This is done without drying out the acetone which leaves

unwanted organic residue on the substrate. After the ultrasonication the substrate is blow dried with nitrogen.

- **Isopropanol (IPA) cleaning:** The substrate is ultrasonicated in IPA for 5 minutes and then blow dried with nitrogen. After this the substrate is heated at 160° C for about 5 minutes to ensure that it is free of moisture or any other volatile compound.

3.1.2 Deposition Methods

Three systems were used to deposit the thin films: Thermal evaporator, Electron beam evaporator and Magnetron sputtering system.

Thermal Evaporation

It is the simplest physical vapour deposition technique. The material to be deposited is placed in tungsten boats. The whole setup is inside a high vacuum chamber. High current is passed through the tungsten boat till it heats up to boil the material. Vapours of the material condense on substrate which placed directly above the boat.

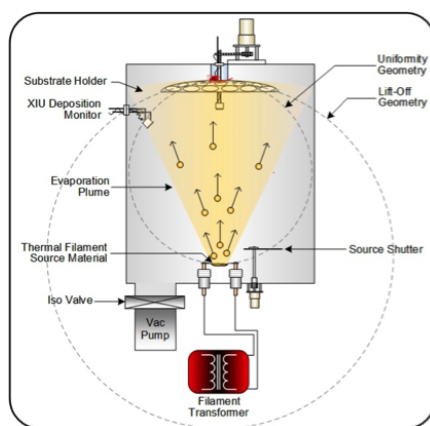


Figure 3.1: Schematic of a standard Thermal evaporation system

Image Source: www.semicore.com

The rate of deposition is monitored using a 6 MHz quartz crystal oscillator. This is very useful to deposit elemental metals.

Copper, aluminium and titanium thin films were deposited using this method.

Electron-beam Evaporation

It is another form of physical vapour deposition. The material to be deposited is placed in a crucible and bombarded with an electron beam, produced and accelerated in an accelerated in an electron gun. The beam is focused onto the target material with the help of controllable magnetic fields. The high kinetic energy of the electrons heats up the material enough to evaporate it.

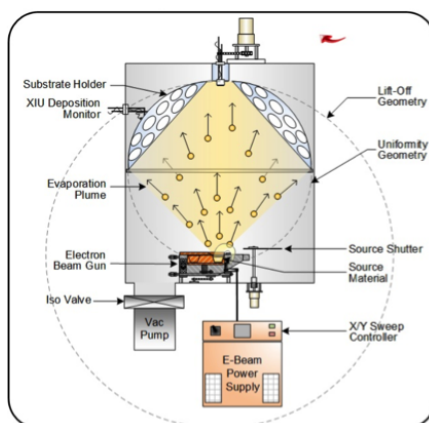


Figure 3.2: Schematic of a standard E-beam evaporation system

Image Source: www.semicore.com

The substrate is placed directly about the target anode and deposition rate is monitored using a 6 MHz quartz crystal oscillator.

This method was used to deposit thin films of silicon, tantalum and niobium.

Reactive Evaporation

The two evaporation methods described above can be modified to deposit certain materials like oxides. This can be done by introducing the gas, which you want to your metal to react with, into the vacuum chamber. The reaction takes place during the condensation of the evaporated metal. The degree of reaction on the ratio of the number of gas molecules to the number of metal atoms hitting the substrate surface. Thus this process needs to be carried out at relatively high partial pressure of the gas and low rates of metal deposition [22] The reaction can be further assisted by creating a plasma of the reactive gas.

Thin films of oxides of aluminium [22], silicon [23] and aluminium/silicon alloy were deposited using reactive evaporation. To deposit AlO_x different methods were tried:

- Continuous evaporation of Al in O₂ environment.
- Depositing a very thin layer of Al and oxidizing it by venting the vacuum chamber with O₂/air.
- A thin nucleation layer of TiO_x was deposited before depositing AlO_x as it is reported that it increases the dielectric constant [24].

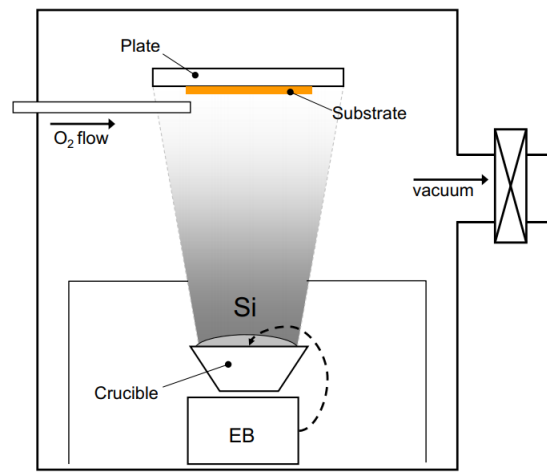


Figure 3.3: Schematic of deposition of SiO₂ by a reactive e-beam evaporation [23].

Reactive ion sputtering

Magnetron Sputtering is a process in which a plasma (glow discharge) is created and positively charged ions from the plasma are accelerated by an electrical field superimposed on the cathode or "target". A discharge is maintained between the anode and the cathode at a pressure of around 10⁻² Torr, and target atoms eject from the bombarded cathode and condense on a suitably placed substrate. Noble gases like argon which do not react with metals are used to deposit metallic films. When a material like alumina (Al₂O₃) is sputtered this way it loses some oxygen (decomposition) upon plasma bombardment. By replacing the inert argon atmosphere with an argon-oxygen mixture, a reactive sputtering system is obtained which allows the deposition of an oxide on the substrate [25]. Aluminum oxide film can also be deposited by sputtering an Al target with argon-oxygen mixture [26].

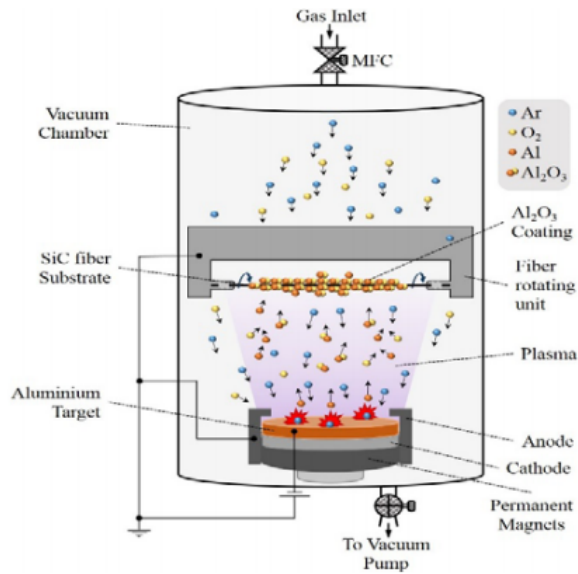


Figure 3.4: Schematic of deposition of Al_2O_3 by a reactive sputtering of Al reported by Palaniyappan et al [26].

3.1.3 Design

Two different designs were used for the MIM structures. In the first the dielectric film and the top electrode are deposited as circular disks (Fig. 3.5). The radius of the top electrode being smaller than that of the dielectric to ensure that it does not short with the bottom electrode.

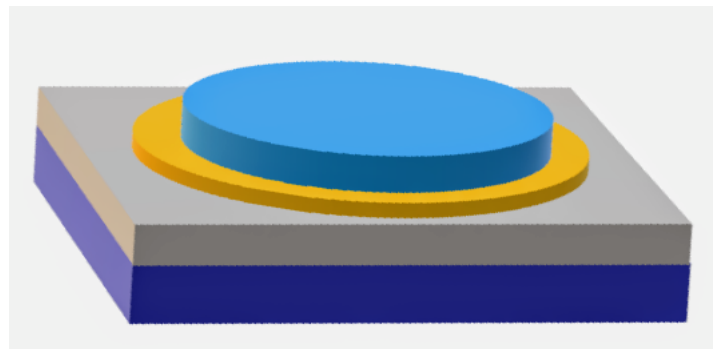


Figure 3.5: Schematic of MIM structure with circular top electrode.

The other design is a cross configuration (Fig. 3.6) such that the contact made on the top electrode wouldn't be directly above the dielectric film. This was done as we wanted to ensure that the dielectric layer wasn't damaged in the process of contacting. Again this was done in such a way as to not short the two electrodes.

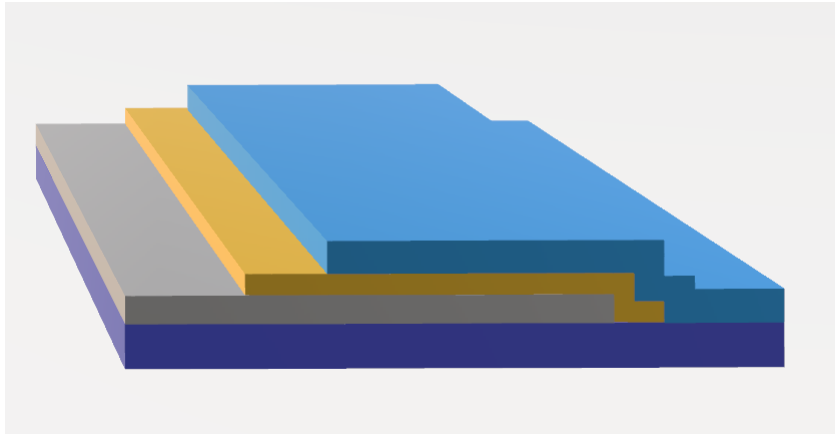


Figure 3.6: Schematic of MIM structure with cross configuration.

3.1.4 Shadow Masking

To achieve the above designs a very simple technique called shadow masking is used. For circular disks stencils with circular holes of the appropriate radius were machined out of iron. Then fixing them very close to the substrate the film deposition was done to get the desired shape of the film.

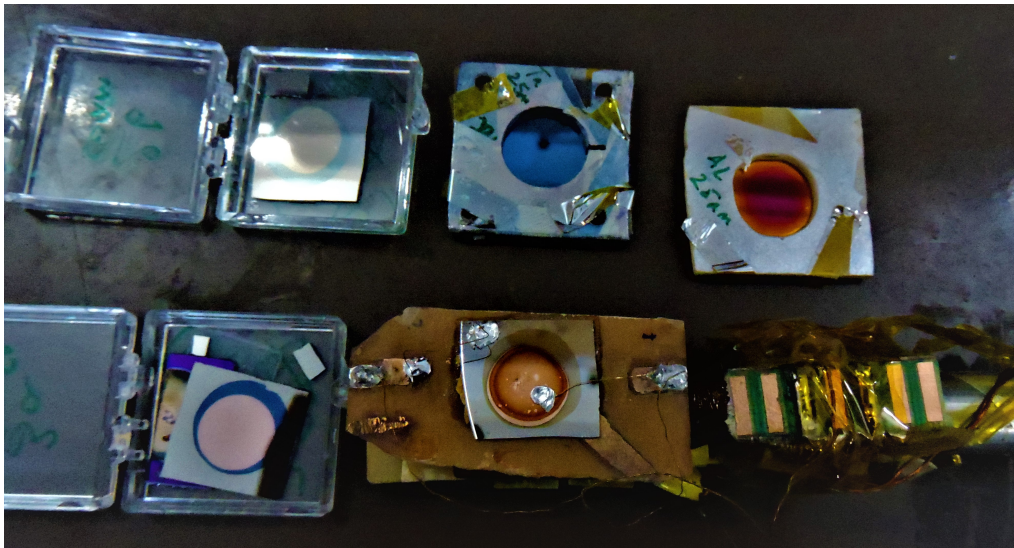


Figure 3.7: MIM structures fabricated by shadow masking with stencils.

For the cross configuration design, Teflon tape is used to mask the regions that are not to be deposited with the film concerned. The Teflon tape is kept in contact with the substrate surface with help bent pins which are used to hold the chips in place when the chip holder is inverted for deposition.



Figure 3.8: Shadow masking with Teflon tape.

3.1.5 Electron-beam lithography

Some samples were also fabricated using e-Beam lithography by Shelender Kumar. This is done by scanning a focused beam of electrons to draw desired shapes on a substrate surface coated with an electron-sensitive film of resist (exposing). The electron beam changes the solubility of the resist, enabling selective removal of either the exposed (positive resist) or non-exposed regions (negative resist) of the resist by developing it in the appropriate solvent.

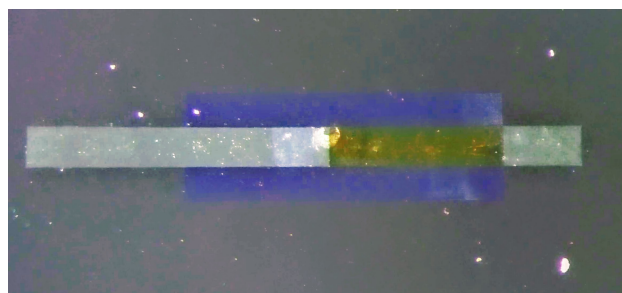


Figure 3.9: MIM structure fabricated in cross configuration using e-beam lithography.

3.1.6 Contacts

Gold wires were used to contact the metal electrodes to the PCB. Two different methods were tried out for the same.

Indium Bonding

Indium has a relatively low melting point of 157°C and is highly malleable. One end of the gold wire is dipped in molten indium and taken out so that a small bulb of indium forms on this end. Then using a sharp wooden toothpick wrapped in Teflon tape, this bulb is gently pressed against the metal surface till the bulb of indium flattens to form a very secure bond to the metal surface. The other end of the gold wire is pressed into a globule of indium which is placed on the contact pad of the PCB. A MIM contacted with indium is shown in Fig. 3.7

Silver Paste Bonding

This is done by simply dipping one end of the gold wire in silver paste and placing it on the metal surface. Then it is allowed to dry out at room temperature or slightly elevated temperature till a secure bond is achieved. The other end can then be soldered to the contact pad using a solder alloy with a low melting temperature as high temperatures can melt the gold wire.

3.2 Measurements

3.2.1 Leakage Current

If the dielectric film is not insulating, it leaks current through it. Using a Keithley 2400 SourceMeter the leakage current is measured by applying voltage of the order mV. If the dielectric film is insulating then we would expect a leakage current of order less than nA (which appears as white noise around 0 A) and a resistance of the order of $\text{G}\Omega$.

3.2.2 Impedance Measurement

Once we have ensured that the dielectric film is insulating we proceed to make impedance measurements on the sample. This is done with the help of Solarton 1260 Impedance/Gain-Phase Analyzer. This makes use of an internal capacitance bridge and outputs phase and real and imaginary capacitance and impedance. These are done at low voltage levels to assure linearity [10].

Chapter 4

Observations and Conclusions

Samples which used thin layer of Si as the dielectric were found to be leaky at both room temperature and at 77K (liquid N₂ boiling point). This could be because of diffusion of Si into the metal electrodes like Cu, Al.

Samples with AlO_x as the dielectric layer were made using different approaches as mentioned in the previous chapter. AlO_x film made by oxidizing thin Al films in air or O₂ environment leaked current. In this method there is little control over the thickness of the oxide film formed. AlO_x films deposited using reactive evaporation was found to be insulating in some samples with small area fabricated using EBL. Fig. 4.1 shows the impedance as a function of frequency with V_{AC} = 0.1 mV and Fig. 4.2 shows the measured capacitance as a function of the AC voltage at 1 kHz frequency.

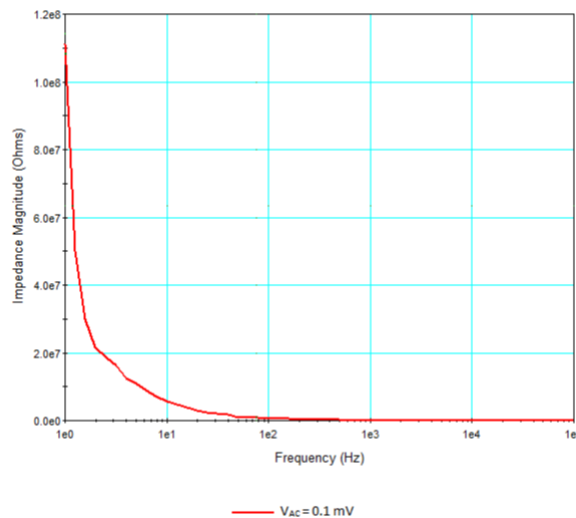


Figure 4.1: Impedance vs Frequency for MIM fabricated with AlO_x film as the dielectric.

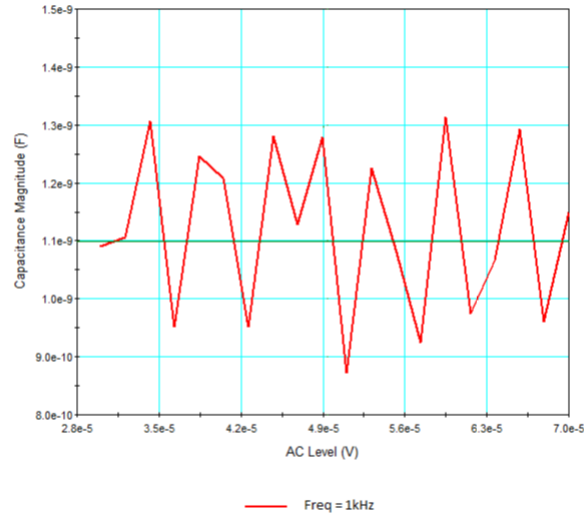


Figure 4.2: Capacitance vs AC Voltage for MIM with AlO_x film as the dielectric.

However AlO_x in samples with a large area ($> 1 \text{ cm}^2$) leaked current. This is possibly due to the non-uniform deposition of AlO_x on the substrate which might be resolved using a revolving substrate holder.

We have also been able to fabricate samples with insulating films of SiO_x deposited using reactive evaporation.

Bibliography

- [1] S. Datta, *Electronic transport in mesoscopic systems*. Cambridge university press, 1997.
- [2] M. Kaplit and J. Zemel, “Capacitance observations of landau levels in surface quantization,” *Physical Review Letters*, vol. 21, no. 4, p. 212, 1968.
- [3] S. Takaoka, K. Oto, H. Kurimoto, K. Murase, K. Gamo, and S. Nishi, “Magnetocapacitance and the edge state of a two-dimensional electron system in the quantum hall regime,” *Physical review letters*, vol. 72, no. 19, p. 3080, 1994.
- [4] A. Widom and T. Clark, “Thermodynamic equations for gate charge storage on a field effect transistor,” *Journal of Physics D: Applied Physics*, vol. 15, no. 12, p. L181, 1982.
- [5] S. Kravchenko, V. Pudalov, and S. Semenchinsky, “Negative density of states of 2d electrons in a strong magnetic field,” *Physics Letters A*, vol. 141, no. 1-2, pp. 71–74, 1989.
- [6] C. Kittel, P. McEuen, and P. McEuen, *Introduction to solid state physics*. Wiley New York, 1996, vol. 8.
- [7] A. Efros, F. Pikus, and V. Burnett, “Thermodynamic density of states of two-dimensional electron gas in a strong magnetic field,” *Solid state communications*, vol. 84, no. 1-2, pp. 91–94, 1992.
- [8] Y. Fukuda, Y. Otani, H. Toyota, and T. Ono, “Electrical characterization techniques of dielectric thin films using metal–insulator–metal structures,” *Japanese Journal of Applied Physics*, vol. 46, no. 10S, p. 6984, 2007.

- [9] S. Mizusaki, T. Miyatake, N. Sato, I. Yamamoto, M. Yamaguchi, M. Itou, and Y. Sakurai, "Electron momentum density and the fermi surface of β -pd h 0.84 by compton scattering," *Physical Review B*, vol. 73, no. 11, p. 113 101, 2006.
- [10] A. Hebard, S. Ajuria, and R. Eick, "Interface contribution to the capacitance of thin-film al-al₂O₃-al trilayer structures," *Applied physics letters*, vol. 51, no. 17, pp. 1349–1351, 1987.
- [11] K. T. McCarthy, A. Hebard, and S. Arnason, "Magnetocapacitance: Probe of spin-dependent potentials," *Physical review letters*, vol. 90, no. 11, p. 117 201, 2003.
- [12] C. Mead, "Anomalous capacitance of thin dielectric structures," *Physical Review Letters*, vol. 6, no. 10, p. 545, 1961.
- [13] J. Krupski, "Interfacial capacitance," *physica status solidi (b)*, vol. 157, no. 1, pp. 199–207, 1990.
- [14] S. Zhang, "Spin-dependent surface screening in ferromagnets and magnetic tunnel junctions," *Physical review letters*, vol. 83, no. 3, p. 640, 1999.
- [15] J. Hirsch, "Metallic ferromagnetism without exchange splitting," *Physical Review B*, vol. 59, no. 9, p. 6256, 1999.
- [16] K. Kim, U. Yu, and B. Min, "Magnetocapacitance in a metal-oxide-metal junction system," *JOURNAL-KOREAN PHYSICAL SOCIETY*, vol. 48, no. 4, p. 599, 2006.
- [17] K. Kim, U. Yu, B. H. Kim, and B. Min, "Effects of band broadening and shape of the density of states on the magnetic phase diagram," *Journal of Physics: Condensed Matter*, vol. 18, no. 31, p. 7227, 2006.
- [18] H. Jamieson and F. Manchester, "The magnetic susceptibility of pd, pdh and pdd between 4 and 300 k," *Journal of Physics F: Metal Physics*, vol. 2, no. 2, p. 323, 1972.
- [19] M. C. Steele, J. W. Hile, and B. A. MacIver, "Hydrogen-sensitive palladium gate mos capacitors," *Journal of Applied Physics*, vol. 47, no. 6, pp. 2537–2538, 1976.
- [20] A. Salomonsson, M. Eriksson, and H. Dannetun, "Hydrogen interaction with platinum and palladium metal–insulator–semiconductor devices," *Journal of Applied Physics*, vol. 98, no. 1, p. 014 505, 2005.

- [21] K. Kim and B. Min, "Magnetocapacitance in a ferromagnetic metal tunnel junction system," *Journal of applied physics*, vol. 101, no. 9, 09G507, 2007.
- [22] K. Kerner, "On the influence of oxygen and water vapour on the reactive condensation of metal oxides," *Japanese Journal of Applied Physics*, vol. 13, no. S1, p. 463, 1974.
- [23] H. Takezawa, K. Iwamoto, S. Ito, and H. Yoshizawa, "Electrochemical behaviors of nonstoichiometric silicon suboxides (siox) film prepared by reactive evaporation for lithium rechargeable batteries," *Journal of power sources*, vol. 244, pp. 149–157, 2013.
- [24] B. Fallahazad, K. Lee, G. Lian, S. Kim, C. Corbet, D. Ferrer, L. Colombo, and E. Tutuc, "Scaling of Al_2O_3 dielectric for graphene field-effect transistors," *Applied Physics Letters*, vol. 100, no. 9, p. 093112, 2012.
- [25] D. Campbell, "2.7 deposition methods for dielectric films and their electrical properties," *Vacuum*, vol. 27, no. 4, pp. 213–225, 1977.
- [26] S. Palaniyappan, P. Chennam, M. Trautmann, H. Ahmad, T. Mehner, T. Lampke, and G. Wagner, "Fabrication and characterization of Al_2O_3 based electrical insulation coatings around SiC fibers," *International Journal of Materials and Metallurgical Engineering*, vol. 13, no. 4, pp. 180–184, 2019.